Molecularly engineered photocatalyst sheet for scalable solar formate production from carbon dioxide and water

Qian WANG,[1] Julien WARNAN,[1] Santiago RODRÍGUEZ-JIMÉNEZ,[1] Jane J. LEUNG,[1] Shafeer KALATHIL,[1] Virgil ANDREI,[1] Kazunari DOMEN,[2,3] Erwin REISNER[1,*]

Affiliation and full postal address

1 *Department of Chemistry, University of Cambridge, Lensfield Road, Cambridge CB2 1EW, UK*

2 *Office of University Professor, The University of Tokyo, 7-3-1 Hongo, Bunkyo-ku, Tokyo 113-8656, Japan*

3 *Research Initiative for Supra-Materials, Interdisciplinary Cluster for Cutting Edge Research, Shinshu University, 4-17-1 Wakasato, Nagano-shi, Nagano 380-8553, Japan*

***Corresponding author**

Professor Erwin REISNER

Department of Chemistry, University of Cambridge, Lensfield Road, Cambridge CB2 1EW, UK

Tel: +44-1223336323

E-mail: reisner@ch.cam.ac.uk

Abstract

Harvesting solar energy to convert CO_2 into chemical fuels is a promising technology to curtail the growing atmospheric CO_2 levels and alleviate the global dependence on fossil fuels. However, the assembly of efficient and robust systems for the selective photoconversion of CO_2 without sacrificial reagents and external bias remains a challenge. Here, we present a photocatalyst sheet that converts CO_2 and H_2O into formate and O_2 as a potentially scalable technology for CO_2 utilisation. This technology integrates La and Rh-doped $SrTiO_3$ ($SrTiO_3$:La,Rh) and Mo-doped $BiVO_4$ ($BiVO_4$:Mo) light absorbers modified by phosphonated Co(II) bis(terpyridine) and RuO_2 catalysts onto a gold layer. The monolithic device provides a solar-to-formate conversion efficiency of 0.08±0.01% with a selectivity for formate of 97±3%. As the device operates wirelessly and uses water as an electron donor, it offers a versatile strategy toward scalable and sustainable CO_2 reduction using molecular-based hybrid photocatalysts.

Coordination complexes have long been explored for achieving the (electro)chemical CO_2 reduction reaction (CO_2RR) and high selectivity with good durability has been reported in homogenous solution.[1, 2] Hybrid systems employ immobilised molecular catalysts on the surface of a semiconductor, which allows their use in a range of solvents for efficient photocatalysis, including an aqueous medium.[3-8] Ultimately, CO_2RR requires coupling with sustainable oxidation chemistry of an abundant electron source such as water for such technologies to satisfy global energy demands.[9] Therefore, particular effort has been focused on the development of standalone hybrid photoelectrochemical (PEC) cells, which can also couple CO_2RR with water oxidation.[10-14] However, hybrid PEC cells suffer from scale-up problems due to the pH gradient and *IR* drops occurring during the PEC reaction.[15]

Colloidal systems using particulate photocatalysts are an emerging alternative to PEC configurations as they benefit from a simpler design and potentially lower cost.[16] However, sacrificial reductants are commonly required for CO_2 conversion using hybrid photocatalysts due to the low oxidising power of the utilised photosensitiser unit, which cannot catalyse water oxidation.[7, 17-19] A nature-inspired artificial Z-scheme CO_2 conversion system composed of a hybrid photocatalyst for CO_2RR and a semiconductor photocatalyst for water oxidation could in principle cope with both the high selectivity of CO_2RR and strong oxidation power. Nonetheless, the realisation of photosynthetic Z-scheme CO_2RR systems remains a critical scientific challenge due to inefficient interparticle charge transfers as well as fiercely competitive side and back reactions such as proton reduction and oxidation of the products from CO_2RR.[20-22] To our knowledge, selective Z-scheme CO_2RR system based on particulate hybrid photocatalysts has yet to be reported.[23]

Z-scheme-inspired photocatalyst sheets consist of two redox-complementary semiconductor particles fixed on a conductive layer that ensures charges relay while avoiding the side reactions associated with the use of redox mediators.[24] As the reduction and oxidation reactions occur in close

proximity to one another on the photocatalyst sheet, the pH gradient and *IR* drop are largely suppressed.[15] The photosynthetic activity of the photocatalyst sheet is thus scalable and avoids PEC limitations.

Here, we report such a monolithic device, taking the $SrTiO_3$:La,Rh|Au|RuO_2-$BiVO_4$:Mo sheet as an example, and immobilise a phosphonated cobalt(II) bis(terpyridine) molecular catalyst as CO_2 reduction catalyst on the surface in a straightforward manner. Solar irradiation of the device delivered formate ($HCOO^-$) from aqueous CO_2 with 97±3% selectivity, accompanied by a simultaneous O_2 generation in a stoichiometric 2:1 ratio with a solar-to-formate conversion efficiency (STF) of 0.08±0.01%. When the sheet device is irradiated with simulated sunlight, electron-hole pairs are excited in both $SrTiO_3$:La,Rh and $BiVO_4$:Mo. Electrons are transferred from the conduction band of $BiVO_4$:Mo to the donor levels of $SrTiO_3$:La,Rh through the gold (Au) layer. Simultaneously, electrons in $SrTiO_3$:La,Rh reduce CO_2 to $HCOO^-$ with the aid of the molecular complex functioning as a CO_2RR cocatalyst, and holes in $BiVO_4$:Mo oxidise water to oxygen with RuO_2 species serving as an oxygen evolution cocatalyst.

Device preparation and characterisation

The photocatalyst sheet, $SrTiO_3$:La,Rh|Au|RuO_2-$BiVO_4$:Mo, consisting of $SrTiO_3$:La,Rh and RuO_2-modified $BiVO_4$:Mo (RuO_2-$BiVO_4$:Mo) particles embedded into a Au layer, was prepared by a previously reported particle transfer method.[25] RuO_2-$BiVO_4$:Mo is expected to provide strong water oxidation power under visible light irradiation,[26] whereas $SrTiO_3$:La,Rh was chosen as the light absorber for CO_2RR owing to its relatively negative conduction band (–1.1 V versus NHE at pH 7).[27] The sheet was subsequently modified with the molecular CO_2RR cocatalyst (**CotpyP**) by immersion from a methanolic solution. Fully assembled **CotpyP**-loaded $SrTiO_3$:La,Rh|Au|RuO_2-$BiVO_4$:Mo sheets with relatively large active areas (ca. 5.7 cm× 6 cm) could be prepared (Figure

1a,b). Scanning electron microscopy and energy dispersive X-ray spectroscopy (SEM–EDX) mapping confirmed that a Au layer with a thickness of ca. 300 nm supports a particle layer composed of $SrTiO_3$:La,Rh and RuO_2-$BiVO_4$:Mo particles (Figure 1c-h, Supplementary Fig. 1).

Precious-metal-free **CotpyP** was selected as the cocatalyst because this 3d transition metal-based complex can be easily prepared and readily immobilised on porous metal oxide scaffolds via its phosphonate anchoring groups, and was previously used for low-overpotential CO_2RR on a p-type silicon photoelectrode (m-TiO_2|*p*-Si) in an aqueous electrolyte solution.[28] SEM–EDX and X-ray photoelectron spectroscopy (XPS) analyses (Co 2p and N 1s spectra; Supplementary Fig. 2) suggest that the **CotpyP** catalyst molecules were adsorbed on both $SrTiO_3$:La,Rh and RuO_2-$BiVO_4$:Mo particles. No significant changes were observed in the attenuated total reflection infrared (ATR-IR) spectra of **CotpyP** powder and **CotpyP** grafted on the $SrTiO_3$:La,Rh and RuO_2-$BiVO_4$:Mo particles (Supplementary Fig. 3 and Supplementary Table 1), indicating an unchanged core structure of the catalyst upon immobilisation. The loading amount of **CotpyP** was estimated via inductively coupled plasma optical emission spectrometry (ICP-OES) to be ~17 nmol cm^{-2} (Supplementary Table 2).

Performance for photosynthetic CO_2RR and water oxidation

Simultaneous production of $HCOO^-$ and O_2 occurred over the **CotpyP**-loaded $SrTiO_3$:La,Rh|Au|RuO_2-$BiVO_4$:Mo sheets (ca. 1 cm^2) in a CO_2-saturated $KHCO_3$ aqueous solution (0.1 M, pH 6.7) under a CO_2 atmosphere (1 atm) and simulated solar irradiation (AM 1.5G, 100 mW cm^{-2}), as shown in Figure 2a. The hybrid photocatalyst sheet enabled an STF of 0.08±0.01%, while attaining 97±3% selectivity for $HCOO^-$ formation. The pH of the reaction medium did not change after 6 hours of irradiation. No products were obtained in the absence of light or either of the semiconductor powders afforded under the same conditions (Supplementary Table 3). These

results supported the occurrence of a Z-scheme mechanism in the sheet system, ruling out the possibilities of significant reduction/oxidation of impurities as sacrificial reagents.

During control experiments performed in an aqueous K_2SO_4 solution (0.1 M, pH 6.7) without CO_2/HCO_3^- and purged with N_2, no CO_2RR products were detected. Continuous H_2 and O_2 with trace amounts were observed and the amount of H_2 was similar to that produced in the presence of CO_2/HCO_3^- (Supplementary Fig. 4 and Supplementary Table 3). These observations indicate that first the H_2 detected from the present sheet was produced via water splitting rather than $HCOO^-$ decomposition and, second, highlight the modest catalytic activity of **CotpyP** for hydrogen production.[28]

Isotopic labelling experiments confirmed that $HCOO^-$ resulted from $^{13}CO_2/H^{13}CO_3^-$ (a doublet attributable to the ^{13}C-coupled proton ($^1J_{CH}$ = 195 Hz) was observed by proton nuclear magnetic resonance (^{1}H NMR) spectroscopy; Figure 2b). The amount of $H^{13}COO^-$ was quantified as 5.3 μmol and comparable to that of the formate obtained from normal $^{12}CO_2/H^{12}CO_3^-$ conditions (Supplementary Table 3). The evolution of O_2 gas accompanied the reduction reactions in a stoichiometric ratio of $(HCOO^-+H_2+CO):O_2$ = 2.2±0.2 ($HCOO^-:O_2$ = 2.1±0.3), demonstrating a clean conversion without the need of sacrificial reagents.

In agreement with absorption onsets of both $SrTiO_3$:La,Rh and $BiVO_4$:Mo in the diffuse reflectance spectra (DRS), $HCOO^-$ was produced up to $\lambda \leq 510$ nm irradiation (Figure 2c), indicating that the photoreactions proceeded via bandgap transitions in the semiconductors. The apparent quantum yield (AQY) at 420±15 nm was 2.6%. A sheet with an active irradiated area of ca. 20 cm^2 was prepared and produced $HCOO^-$ with an STF of 0.06% (Figure 3), which is comparable to those detected from the 1 cm^2 samples (Figure 2a), demonstrating the scalability of our photocatalyst sheet system.

The photocatalyst particles covered more than 90% of the underlying Au layer (Figure 1h) and the exposed Au did not show significant activity for electrocatalytic CO_2RR (Supplementary Fig. 5). Furthermore, the **CotpyP**-loaded Au film yielded no detectable products without applied potential, while the $SrTiO_3$:La,Rh|Au|RuO_2-$BiVO_4$:Mo sheet without **CotpyP** produced negligible $HCOO^-$ (Supplementary Table 3). The Au layer is thus believed to serve only as an electron transfer medium between $SrTiO_3$:La,Rh and $BiVO_4$:Mo rather than as a catalyst for CO_2RR.

Photocatalytic reactions over the colloidal systems, in which individual semiconductor powders were suspended in aqueous solution containing sacrificial reagents, were carried out to ascertain the function of **CotpyP** (Supplementary Table 4). Upon loading of **CotpyP** on $SrTiO_3$:La,Rh, $HCOO^-$ production became evident in the presence of triethanolamine (TEOA) as an electron donor, confirming the function of **CotpyP** as the CO_2RR cocatalyst. The turnover number (TON) for $HCOO^-$ was 305 after 4 hours. Likewise, photocurrent over the **CotpyP**-modified $SrTiO_3$:La,Rh|Au photocathode for CO_2RR increased remarkably compared to the pristine $SrTiO_3$:La,Rh photocathode (Figure 4a). In contrast, O_2 evolution showed no significant improvement after loading **CotpyP** on either $SrTiO_3$:La,Rh or $BiVO_4$:Mo in an aqueous solution containing Ag^+ as electron acceptor (Supplementary Table 4). Similar photocurrents for the RuO_2-$BiVO_4$:Mo|Au photoanode were also observed with and without loading **CotpyP** on its surface in an electrolyte solution containing $HCOO^-$ (Supplementary Fig. 6). It can therefore be concluded that **CotpyP** serves as a CO_2RR cocatalyst on $SrTiO_3$:La,Rh, and not as an oxygen evolution or formate oxidation cocatalyst on $BiVO_4$:Mo. In addition, the O_2 evolution rate over RuO_2-$BiVO_4$:Mo sheet in a 0.1 M $AgNO_3$ aqueous solution did not show significant change after loading **CotpyP** on its surface (1.2 μmol h^{-1} cm^{-2} and 1.3 μmol h^{-1} cm^{-2} obtained on RuO_2-$BiVO_4$:Mo and **CotpyP**/RuO_2-$BiVO_4$:Mo sheets, respectively), indicating the negligible impact of **CotpyP** on the O_2 evolution rate over RuO_2-$BiVO_4$:Mo. Considering that $BiVO_4$:Mo is unable to produce $HCOO^-$

from CO_2 due to insufficient driving force from its conduction band,[29-31] we propose that $HCOO^-$ and O_2 were therefore generated by two-step photoexcitation over the $SrTiO_3$:La,Rh and $BiVO_4$:Mo particles (Figure 1a).

In order to investigate the robustness of **CotpyP** toward O_2, the controlled potential electrolysis experiments (CPE) of **CotpyP**|m-TiO_2|Ti electrode were performed with and without the presence of O_2 (Figure 5). The Faradaic efficiency for $HCOO^-$ dropped from 83% to 40% when replacing the mixture of CO_2 and N_2 (CO_2+N_2, 50% each) with that of CO_2 and O_2 (CO_2+O_2, 50% each) due to cooccurrence of the oxygen reduction reaction (Figure 5b). However, the amount of $HCOO^-$ produced did not change substantially (16.1 and 13.7 μmol in 5h using a CO_2+N_2 and CO_2+O_2 atmosphere, respectively), implying substantial $HCOO^-$ production activity remained in the presence of O_2 and the O_2 reduction reaction occurred mainly on m-TiO_2|Ti electrode, as evidenced by the red dashed curve in Figure 5a. After re-purging with CO_2+N_2 and repeating linear sweep voltammetry (LSV) scan, a significant drop in the CO_2 reduction activity was not observed, which illustrated the O_2 tolerance of **CotpyP** (Figure 5a).[32]

Device selectivity and stability

To date, reported photo(electro)chemical reduction of aqueous CO_2 to a single product using molecular catalysts remains scarce, in particular due to the competing proton reduction reaction. For instance, **CotpyP**-loaded m-TiO_2|*p*-Si poised at an applied potential of 0 V versus reversible hydrogen electrode (RHE) favoured PEC H_2 production instead of CO_2 reduction.[28] To investigate the factors influencing the selectivity of **CotpyP**, the PEC performance of a **CotpyP**-loaded $SrTiO_3$:La,Rh photocathode for CO_2RR was studied in a CO_2-saturated $KHCO_3$ aqueous solution (0.1 M, pH 6.7) under a CO_2 atmosphere (1 atm) and simulated solar irradiation (AM 1.5G, 100 mW cm^{-2}). Under 0.0 V versus RHE applied potential in the controlled potential photoelectrolysis

(CPPE), more H_2 than CO and $HCOO^-$ was produced over **CotpyP**-$SrTiO_3$:La,Rh (Figure 4b and c), consistent with results on **CotpyP**-m-TiO_2|*p*-Si. The **CotpyP**-$SrTiO_3$:La,Rh|Au achieved a higher total TON and selectivity for CO and $HCOO^-$ (144 after 4 h CPPE, 47%) than **CotpyP**-m-TiO_2|*p*-Si (20.8 after 8 h CPPE, 37%),[28] presumably due to the more negative conduction band potential of $SrTiO_3$:La,Rh than that of TiO_2 (–1.1 and –0.5 V versus NHE at pH 7 for $SrTiO_3$:La,Rh and TiO_2, respectively).

The shared electrode potential, at which the **CotpyP**-$SrTiO_3$:La,Rh|Au and RuO_2-$BiVO_4$:Mo|Au photoelectrodes generate photocathodic and photoanodic currents without external bias, was estimated to be +0.45 V versus RHE (Supplementary Fig. 7). In contrast, $HCOO^-$ became the predominating product with a selectivity of 93±3% (Faradaic efficiency for $HCOO^-$ production was 83.9±5.8% over 4 hours) when the potential was increased to +0.5 V versus RHE (Figure 4b and c). The increasing dominance of hydrogen evolution at higher applied potentials has also previously been observed on **CotpyP**-m-TiO_2|*p*-Si photocathode.[28] The surface reaction pathways and rate-determining steps might change caused by a variation in the photo-charging rate and outer Helmholtz adsorption potential at different applied bias.[33-36] Hence, the photocatalyst sheet can yield $HCOO^-$ with high selectivity. Additionally, a current-increasing effect (caused by the presence of formate as an electron donor) was not observed on a RuO_2-$BiVO_4$:Mo photoanode in the electrolyte containing 1.5 mM $HCOO^-$ (Supplementary Fig. 6), suggesting that the photogenerated holes in RuO_2-$BiVO_4$:Mo selectively oxidise water rather than $HCOO^-$ due to the high activity of RuO_2 for water oxidation.[11,37]

The photosynthetic reaction over the **CotpyP**-$SrTiO_3$:La,Rh|Au|RuO_2-$BiVO_4$:Mo sheet was carried out for 24 hours with the replacement of the reactant medium with a fresh solution and CO_2 purging every 6 hours (Figure 4d). The $HCOO^-$ and O_2 formation rates remained at 51% of the initial activity after 24 hours. The X-ray diffraction (XRD) patterns of the sheet before and after

reaction (Supplementary Fig. 8) showed that the phases of $SrTiO_3$:La,Rh, $BiVO_4$:Mo and Au did not change notably. Additionally, no notable peak shift was observed in Co 2p and N 1s XPS spectra (Supplementary Fig. 2), suggesting that no significant heterogenisation of **CotpyP** occurred during the reaction. A small peak attributable to hydrous ruthenium oxide was observed along with the major peak of RuO_2 after the 24-hour reaction conducted in aqueous solution.

While the amount of Ru remaining on the photocatalyst sheet did not remarkably decrease, that of Co dropped by half after the 24-hour reaction (Supplementary Table 2). Accordingly, the TONs for $HCOO^-$ in the first and fourth runs were calculated to be 428 and 447, respectively. Note that these values are conservative estimates for the TONs because the **CotpyP** deposited on $BiVO_4$:Mo was inactive for the CO_2RR and other leaching/inactive Co was not taken into account. The comparable TON in the last run compared with the initial one further confirmed that the function of the residual **CotpyP** cocatalyst was preserved.

Reported systems coupling CO_2RR with water oxidation for formate production remain scarce, whether in powder suspension form or bias-free PEC cells. A wired system consisting of a ruthenium complex-modified N,Zn-Fe_2O_3 photocathode and a photoanode based on n-type $SrTiO_{3-x}$ single crystal was reported to produce 1.55 μmol $HCOO^-$ after 1 hour when the complex loading amount was 70 nmol, corresponding to a TON for $HCOO^-$ of 22.[38] The reaction rate of the present sheet system was recovered to 80% of the initial rate by reloading the **CotpyP** cocatalyst, suggesting the decrease of the activity is attributable mainly to the drop in the number of active sites rather than the essential deterioration of the sheet structure. In the future, the efficiency and durability of the present sheet could be upgraded through improvement in the molecular cocatalyst, such as replacing phosphonate with a more robust anchoring group or constructing a polymeric matrix,[39] and grafting the molecular cocatalysts on the surface of CO_2RR photocatalysts selectively by photoreduction.[40]

Due to the unique structure of photocatalyst sheet, the pH gradient and *IR* drop between the $SrTiO_3$:La,Rh and $BiVO_4$:Mo generated during the redox reactions can be effectively suppressed.[15] As a consequence, the photocatalyst sheet was five times more active than a conventional bias-free PEC parallel cell consisting of a **CotpyP**-$SrTiO_3$:La,Rh photocathode and a RuO_2-$BiVO_4$:Mo photoanode under the same conditions (Supplementary Fig. 9). The photocatalyst sheet design is particularly beneficial to the molecularly-engineered system because it can be used in the aqueous solution with a wide range of pH (2.5–7.5).[41] Therefore, various molecular catalysts could be applied to the photocatalyst sheet in future development. In addition, precious-metal-free photocatalyst sheets with a large area can be readily established by replacing the gold with sputtered carbon or indium tin oxide nanoparticles.[15,24] Hence, this technology displays promising efficiency as well as advantageous versatility and scalability for combing molecular catalysts and semiconductors to achieve artificial photosynthesis.

Conclusions

We demonstrate a hybrid prototype photocatalyst sheet performing photosynthetic CO_2RR to form $HCOO^-$ with a selectivity of 97±3% and an STF of 0.08±0.01% using water as the electron donor. This performance is achieved due to the combined high selectivity of an immobilised precious-metal-free molecular catalysts for CO_2RR and the strong water oxidation power of the semiconductors. The present wireless and stand-alone device couples formate production with water oxidation using light as the sole energy source, a rarity in the field of wireless CO_2 conversion. It also shows high stability during the photosynthetic reaction without sacrificial reagents and enables the scalability of the photocatalytic activity. This finding overcomes the hurdle of hybrid photocatalysts requiring sacrificial reagents in photocatalytic CO_2RR constructs and provides the impetus to study other molecular catalysts for solar fuel production via artificial photosynthesis in

such an architecture. Although here we focus on production of formic acid – a promising fuel and H_2 carrier – the simplicity of the assembly process for immobilising molecular catalysts on the photocatalyst sheet allows the exploration of a wide range of catalysts for various photosynthetic reactions and products in the future.

Methods

Synthesis of $SrTiO_3$:La,Rh and $BiVO_4$:Mo powders

$SrTiO_3$:La,Rh (La/(La + Sr) = Rh/(Rh + Ti) = 4 mol%) was synthesised by a two-step solid-state reaction according to a previously reported procedure.[24] In the initial step, $SrCO_3$ (Alfa Aesar, 99.99%, heated in air at 573 K for 1 h before use) and rutile-type TiO_2 (Sigma-Aldrich, ≥99.98%) powders were mixed in a mortar at a Sr/Ti ratio of 1.05. The mixture was placed into an alumina crucible, heated up to 1473 K at 10 K min^{-1}, and kept at the target temperature for 10 h. The sample was allowed to cool naturally to room temperature. Subsequently, the resulting $SrTiO_3$ was mixed with La_2O_3 (La/(La + Sr) = 4 mol%; Fisher Scientific, 99.99%, freshly calcined in air at 1273 K for 12 h before use) and Rh_2O_3 (Rh/(Rh + Ti) = 4 mol%; Wako Pure Chemical, 98.0–102.0%), and heated at 1373 K for 6 h. The heating and cooling procedures were carried out in the same way as the first step.

$BiVO_4$:Mo (Mo/V = 0.05 mol%) was synthesised via a solid-liquid reaction.[42] Layered Mo-doped $K_3V_5O_{14}$ was prepared as a precursor by calcining a mixture of K_2CO_3 (Breckland Scientific, 99.5%), V_2O_5 (Fisher Scientific, 99.6%) and MoO_3 (Mo/V = 0.05 mol%, BDH Chemicals, 99.5%) in air at 723 K for 5 h. Then, the obtained Mo-doped $K_3V_5O_{14}$ was added to a suspension of $BiONO_3$ (adding stoichiometric $Bi(NO_3)_3 \cdot 5H_2O$ (Sigma-Aldrich, 98%) in 100 mL distilled water) and stirred mildly at 343 K for 10 h. The resulting powder was collected by filtration, washed with distilled water and then dried overnight in air before use.

Loading of RuO_2 on $BiVO_4$:Mo powders

RuO_2, determined by XPS (Supplementary Fig. 2) as an oxygen evolution cocatalyst, was loaded on $BiVO_4$:Mo particles in advance of the sheet preparation. RuO_2 nanoparticles (1 wt%) were loaded on $BiVO_4$:Mo by following an impregnation method.[26] $BiVO_4$:Mo powder (0.1–0.2 g) was immersed in an aqueous solution containing a given amount of $RuCl_3$ (Acros Organics, 35–40% Ru) and placed in a water bath. After evaporating the solution to dryness, the resulting powder was collected and calcined in air at 623 K for 1 h.

Fabrication of $SrTiO_3$:La,Rh|Au|RuO_2-$BiVO_4$:Mo sheets

$SrTiO_3$:La,Rh|Au|RuO_2-$BiVO_4$:Mo photocatalyst sheets were fabricated by a particle transfer method.[24,25] First, a mixture of $SrTiO_3$:La,Rh and RuO_2-loaded $BiVO_4$:Mo powders (10 mg each) was suspended in isopropanol (Sigma-Aldrich, ≥99.5%, 0.5 mL) by ultrasonication for 20 min and drop-cast on a glass substrate (3 cm × 3 cm). After drying at room temperature, a gold layer was deposited by thermal vacuum evaporation (Kurt J. Lesker) under a base pressure below 5×10^{-3} Pa. The thickness of ca. 300 nm of the gold layer was controlled by a crystal sensor and a thickness monitor. The obtained sample was placed on an alumina plate, heated to 573 K under air at a rate of 10 K min^{-1}, and kept at the target temperature for 20 min to form good contact between gold and semiconductors.[24] This process would damage the **CotpyP** and thus the molecular cocatalyst was deposited on the surface after the assembly of the photocatalyst sheet. The Au film supporting the particulate photocatalysts was then bonded to a second glass plate (1 cm × 1 cm unless otherwise noted) with adhesive carbon tape and then lifted off the primary glass plate. Finally, the photocatalyst sheet obtained was ultrasonicated twice, for 2 min each time, in distilled water to remove excess particles piling up on the particle layer.

Assembly of CotpyP on $SrTiO_3$:La,Rh|Au|RuO_2-$BiVO_4$:Mo sheets

A methanolic solution of **CotpyP** (0.25 mM) was prepared by the dropwise addition of a methanol solution of **tpyP** (2,2':6',2"-terpyridine-4'-phosphonic acid, HetCat) to a methanol solution of $Co(BF_4)_2 \cdot 6H_2O$ (Sigma Aldrich, >99%).[28] Ultraviolet-visible (UV-Vis), and ^{1}H NMR spectra are presented in Supplementary Figs. 10 and 11. Immobilisation of **CotpyP** on the $SrTiO_3$:La,Rh|Au|RuO_2-$BiVO_4$:Mo photocatalyst sheet was performed by soaking the sheet in the methanolic solution of **CotpyP** for 10 h. The **CotpyP**-loaded $SrTiO_3$:La,Rh|Au|RuO_2-$BiVO_4$:Mo photocatalyst sheet was then rinsed with methanol and dried for ca. 16 h in air before use.

Fabrication of photoelectrodes and PEC parallel cell

Photoelectrodes of $SrTiO_3$:La,Rh|Au and RuO_2-$BiVO_4$:Mo|Au were prepared by the particle transfer method similar to the fabrication of the photocatalyst sheet. $SrTiO_3$:La,Rh or RuO_2-$BiVO_4$:Mo powder (20 mg) was dispersed in isopropanol (0.5 mL) by ultrasonication for 20 min. The suspension was deposited on a glass substrate (3 cm × 3 cm). Au layers 1.5 μm in thickness were deposited on the semiconductor particles by vacuum evaporation. The resulting Au film holding the photocatalyst powder was annealed at 573 K for 20 min and then transferred to another glass plate (1 cm × 1 cm). Loading of **CotpyP** on $SrTiO_3$:La,Rh|Au and RuO_2-$BiVO_4$:Mo|Au electrodes was carried out by soaking the electrode in the methanolic solution of **CotpyP** as described above for 10 h. The **CotpyP**-loaded photoelectrodes were then rinsed with methanol and dried for ca. 16 h in air. Electrical contact was established by embedding a copper wire in indium at the bottom of the sample. The copper wire and indium were encapsulated with epoxy (Araldite, Rapid 5-Minute Epoxy). The exposed active area of the photoelectrode after the insulation was ~0.2 cm^2.

The **CotpyP**-$SrTiO_3$:La,Rh|Au and RuO_2-$BiVO_4$:Mo|Au electrodes were connected using indium solder to form PEC parallel cells with side-by-side placement of the electrodes. The indium was subsequently covered with epoxy and the exposed area after packaging was about 0.8 cm^2.

Characterisation

XRD patterns of the samples were measured with a PANalytical Empyrean Series 2 instrument using Cu Kα source operated at 40 kV and 40 mA. The DRS were recorded using an ultraviolet-visible-near-infrared spectrometer (Varian Cary 50 Bio). The SEM-EDX element mapping images were obtained using a TESCAN MIRA3 FEG-SEM instrument with an Oxford Instruments Aztec Energy X-maxN 80 system at an acceleration voltage of 15 kV. XPS analysis was carried out at the EPSRC National Facility for Photoelectron spectroscopy ('HarwellXPS') using a Kratos Axis SUPRA XPS fitted with a monochromated Al kα X-ray source (1486.7 eV), a spherical sector analyser, 3 multichannel resistive plate and 128 channel delay line detectors. All data were recorded over a spot size of 700 × 300 μm and at 150 W under a pressure below 10^{-8} Torr and a room temperature of 294 K. Electronic charge neutralisation was achieved using a magnetic immersion lens. Filament current, charge balance and filament bias was 0.27 A, 3.3 V and 3.8 V, respectively. ICP-OES measurements were recorded on a Thermo Scientific iCAP 7400 ICP-OES DUO spectrometer. Analyte solutions for ICP-OES were obtained by digesting the sheets in aqueous HNO_3 (>68%) overnight and dilution to 2% vol/vol with Milli-Q water. FT-IR spectra were collected on a Thermo Scientific Nicolet iS50 FT-IR spectrometer in ATR-IR mode. The ^{1}H NMR spectra of **CotpyP** were recorded in a Bruker 500MHz DCH cryoprobe spectrometer at room temperature. Chemical shifts are given in ppm and are referenced relative to residual protium in the deuterated methanol and deuterium oxide (Eurisotop). Solution UV-vis spectra were collected using

an Edinburgh Instruments FS5 spectrofluorimeter with a quartz cuvette (Starna Scientific) at room temperature.

Photocatalytic reactions

Z-scheme photosynthetic reactions were carried out in a closed system with side illumination from Newport Oriel 67005 solar light simulators with Air Mass 1.5 Global (AM 1.5 G) solar filters, which were calibrated to 100 mW cm^{-2} (1 Sun) using a certified Newport 1916-R optical power meter. A LOT-QD LS0816-H large area solar simulator was employed for the scalability tests. The photocatalyst sheet samples (ca. 1 cm^2) were attached to a steel rod and inserted into the reaction cell containing an aqueous solution of 0.1 M $KHCO_3$ (12 mL) unless otherwise noted. The photosynthetic reactions over the photocatalyst sheet with an active irradiated area of ca. 20 cm^2 were carried out in a custom-built reactor (Figure 3a). Before performing the photosynthetic reaction, the reactant in the cell was purged for 30 min with CO_2 containing 2% CH_4 as an internal standard for gas chromatography (GC) measurements. The pH of the reactant after CO_2 purging was 6.7. CO and H_2 quantification were executed by manual sampling from the headspace of the reaction cells into a Shimadzu GC-2010 Plus gas chromatograph with a barrier discharge ionisation detector. The GC-2010 Plus was equipped with a ShinCarbon micro ST column (0.53 mm diameter) kept at 313 K using a helium carrier gas. Aliquots (50 μL) of the headspace gas were removed from the sealed cell using a gastight syringe (Hamilton, GASTIGHT) for GC analysis. The error for the integrated CH_4 peak area in all injections was 2-3%. In addition, no trend (increase or decrease) was observed on the peak areas during the reaction, indicating that the amount of CH_4 did not undergo significant changes. Formate was analysed by ion chromatography (IC) using a Metrohm 882 Compact IC plus ion chromatography system with a solution of carbonate (4 mM) containing acetone (50 mL L^{-1}) as the eluent. ^{1}H NMR spectroscopy was conducted on a Bruker 400 MHz

NMR spectrometer in D_2O. The O_2 evolution was traced using a NeoFox-GT fluorometer and Fospor-R fluorescence oxygen sensor probe from Ocean Optics inside a glove box with an O_2 concentration of less than 3 ppm. The analytical errors are <5% for quantifying $HCOO^-$, H_2 and CO, and <10% for O_2.

In the colloidal systems for photocatalytic CO_2RR, TEOA was used as an electron donor. $SrTiO_3$:La,Rh powder (2 mg) was added to Pyrex glass photoreactor vials containing an aqueous solution of TEOA (0.1 M, 2 mL) and capped with rubber septa. For the water oxidation reaction, $BiVO_4$:Mo powder (2 mg) was dispersed in 2 mL of an $AgNO_3$ (0.1 M) aqueous solution in the same vials, where Ag^+ cations acted as sacrificial electron acceptors. For the **CotpyP**-$SrTiO_3$:La,Rh and **CotpyP**-$BiVO_4$:Mo samples, 65 μL methanolic solution of **CotpyP** (0.25 mM) was added to the reactant. After briefly vortexing, the samples were purged with CO_2 (for CO_2RR) or N_2 (for water oxidation reaction) containing 2% CH_4 as an internal standard at ambient pressure for 30 min and then irradiated by a solar light simulator (AM 1.5G, 100 mW cm^{-2}).

Error bars in the figures and tables correspond to the standard deviation (n = 3). The source data containing the individual data points used for the statistical analysis are available from the Cambridge data repository.[43]

Photoelectrochemical measurements

The **CotpyP**-$SrTiO_3$:La,Rh|Au and (**CotpyP**/)RuO_2-$BiVO_4$:Mo|Au electrodes were characterised in a three-electrode configuration using a Ag/AgCl reference electrode (in saturated KCl aqueous solution, Basi MW-2030) and a platinum mesh counter electrode. A Selemion (AGC Engineering) was used as the ion-exchange membrane separating the anodic and cathodic compartments. The potential of the working electrode was controlled by a potentiostat (Ivium CompactStat). 0.1 M $KHCO_3$ aqueous solution purged with CO_2 containing 2% CH_4 for 30 min was

used as the electrolyte (pH 6.7) under stirring unless otherwise noted. The photoelectrode was irradiated with a solar simulator (AM 1.5G, 100 mW cm^{-2}). Current-potential curves were measured at a scan rate of 10 mV s^{-1}.

O_2-inhibition of CotpyP catalyst

The preparation of the m-TiO_2|Ti electrode (TiO_2 layer thickness of ~6 μm) was performed following a previously reported procedure.[28] The Ti foil (10 × 20 × 0.25 mm) was sonicated sequentially in isopropanol and ethanol for 30 min, and dried under a flow of N_2. The mesoporous TiO_2 (m-TiO_2) scaffold was deposited on Ti foil by slot-coating commercial Ti-nanoxide pastes (15-20 nm particles, 100 % anatase, Solaronix) over a defined area (0.7 cm × 0.7 cm). The electrodes were then sintered in a Carbolite furnace under atmospheric conditions at 598 K for 5 min, followed by annealing at 648 K for 5 min, and lastly by annealing at 723 K for 5 min.

Immobilisation of **CotpyP** on m-TiO_2|Ti electrode was carried out by soaking the electrodes in a methanolic solution of **CotpyP** (0.25 mM, same solution as that used for photocatalyst sheet) for 16 h.[28] Subsequent electrical contact was established in the same manner used on **CotpyP**-$SrTiO_3$:La,Rh|Au and RuO_2-$BiVO_4$:Mo|Au photoelectrodes.

LSV experiments were carried out in the same three-electrode configuration described above in aqueous $KHCO_3$ solution (0.1 M, pH 6.7) purging with CO_2+N_2 (50% each) or CO_2+O_2 (50% each) for 30 min. The LSV scans were recorded at a scan rate of 50 mV s^{-1} from positive to negative potential. CPE experiments were performed at an applied potential of –0.3 V versus RHE.

Isotopic labelling

The photocatalytic reaction over **CotpyP**-$SrTiO_3$:La,Rh|Au|RuO_2-$BiVO_4$:Mo was performed in 0.1 M $NaH^{13}CO_3$ (Sigma-Aldrich, 98 atom% ^{13}C, 99% (CP)) aqueous solution with $^{13}CO_2$ (Sigma-

Aldrich, 99.0 atom % ^{13}C, 99% (CP)) as the headspace gas. The amount of $HCOO^-$ produced in 6 h was analysed by both IC and ^1H NMR spectroscopy on a Bruker 500 MHz DCH cryoprobe spectrometer at room temperature.

Quantum yield measurements

The AQY of the Z-scheme photocatalytic reaction was calculated using

$$AQY = (4R/I) \times 100\%$$

Where R and I denote the $HCOO^-$ production rate and the photon flux of monochromatic light, respectively. The present system is based on a two-step photoexcitation mechanism. To produce one formate molecule, two electrons in $SrTiO_3$:La,Rh are consumed in the CO_2 reduction reaction, whereas the two electrons are needed in $BiVO_4$:Mo to combine with the holes in $SrTiO_3$:La,Rh to complete the reaction. Therefore, four electrons are required to produce one formate molecule.[44] The AQYs were determined using a LOT MSH-300 monochromator, the power at different wavelengths of which was measured using a Thorlabs PM100D power meter with a Thorlabs S302C thermal power sensor. The wavelength λ with a full width at half maximum of 15 nm was varied between 390 and 540 nm in 30 nm steps.

Solar-to-formate conversion efficiency

The STF is given as

$$STF\ (\%) = (R(HCOO^-) \times \Delta G_r) / (P \times S) \times 100$$

where $R(HCOO^-)$, ΔG_r, P and S indicate the rate of $HCOO^-$ formation during the Z-scheme reaction, the reaction Gibbs energy of the CO_2 reduction reaction (238 kJ mol^{-1}),[31] the energy intensity of the AM 1.5G solar irradiation (100 mW cm^{-2}) and the irradiated sample area, respectively.

Data Availability

The data supporting the findings of the study are available in the paper and its supplementary materials. Source data for the main figures (Figs. 2, 3, 4 and 5) are provided with the paper. Other source data supporting the findings of this study are available from the Cambridge data repository (https://doi.org/10.17863/CAM.54840).

Acknowledgements

We thank Constantin Sahm and Dr. Annika Eisenschmidt at the University of Cambridge for assisting with the isotopic labelling experiment, Dr. Souvik Roy and Dr. Motiar Rahaman at the University of Cambridge for helpful discussions, Stephen Young at the University of Cambridge for performing ICP-OES analysis, and Mark Isaacs at HarwellXPS for carrying out XPS. This work was supported by Marie Sklodowska-Curie individual Fellowships European (to Q.W., GAN 793996 and to S.K., GAN 744317), European Commission Future and Emerging Technologies (FET) Open programme project SoFiA (to S.R.-J. and E.R., GAN 828838), Christian Doppler Research Association (Austrian Federal Ministry for Digital and Economic Affairs and the National Foundation for Research, Technology and Development) and the OMV Group (to J.W. and E.R.). V.A. is grateful for the financial support from the Cambridge Trusts (Vice-Chancellor's Award) and the Winton Programme for the Physics of Sustainability. J.J.L. is supported by the Woolf Fisher Trust in New Zealand. The XPS data collection was performed at the EPSRC National Facility for XPS ("HarwellXPS"), operated by Cardiff University and University College London, under Contract No. PR16195.

Author contributions

Q.W. and E.R. conceived the idea. E.R. supervised the project. J.W., J.J.L. and S.R.-J. synthesised and characterised **CotpyP**. Q.W. prepared the photocatalyst sheet and photoelectrodes and conducted physical characterisations and photo(electro)chemical experiments. S.K. carried out NMR spectroscopy, V.A. assisted with O_2 quantification and scalability tests. All authors analysed the data, discussed the results and assisted with manuscript preparation.

Competing interests

The authors declare no competing interests.

References

1. Costentin, C., Robert, M. & Savéant, J.-M. Catalysis of the electrochemical reduction of carbon dioxide. *Chem. Soc. Rev.* **42**, 2423–2436 (2013).
2. Francke, R., Schille, B. & Roemelt, M. Homogeneously catalyzed electroreduction of carbon dioxide—methods, mechanisms, and catalysts. *Chem. Rev.* **118**, 4631–4701 (2018).
3. Sato, S., Morikawa, T., Saeki, S., Kajino, T. & Motohiro, T. Visible-light-induced selective CO_2 reduction utilizing a ruthenium complex electrocatalyst linked to a p-type nitrogen-doped Ta_2O_5 semiconductor. *Angew. Chem. Int. Ed.* **49**, 5101–5105 (2010).
4. Wang, W.-H., Himeda, Y., Muckerman, J. T., Manbeck, G. F. & Fujita, E. CO_2 hydrogenation to formate and methanol as an alternative to photo- and electrochemical CO_2 reduction. *Chem. Rev.* **115**, 12936–12973 (2015).
5. Kuriki, R. *et al*. Nature-inspired, highly durable CO_2 reduction system consisting of a binuclear ruthenium(II) complex and an organic semiconductor using visible light. *J. Am. Chem. Soc.* **138**, 5159–5170 (2016).

6. Liu, X., Inagaki, S. & Gong, J. Heterogeneous molecular systems for photocatalytic CO_2 reduction with water oxidation. *Angew. Chem. Int. Ed.* **55**, 14924–14950 (2016).

7. Kuriki, R. *et al*. Robust binding between carbon nitride nanosheets and a binuclear ruthenium(II) complex enabling durable, selective CO_2 reduction under visible light in aqueous solution. *Angew. Chem. Int. Ed.* **56**, 4867–4871 (2017).

8. Dalle, K. E. *et al*. Electro- and solar-driven fuel synthesis with first row transition metal complexes. *Chem. Rev.* 119, 2752–2875 (2019).

9. Tu, W., Zhou, Y. & Zou, Z. Photocatalytic conversion of CO_2 into renewable hydrocarbon fuels: state-of-the-art accomplishment, challenges, and prospects. *Adv. Mater.* **26**, 4607–4626 (2014).

10. Sato, S. *et al*. Selective CO_2 conversion to formate conjugated with H_2O oxidation utilizing semiconductor/complex hybrid photocatalysts. *J. Am. Chem. Soc.* **133**, 15240–15243 (2011).

11. Arai, T., Sato, S., Kajino, T. & Morikawa, T. Solar CO_2 reduction using H_2O by a semiconductor/metal-complex hybrid photocatalyst: enhanced efficiency and demonstration of a wireless system using $SrTiO_3$ photoanodes. *Energy Environ. Sci.* **6**, 1274–1282 (2013).

12. Sahara, G. *et al*. Photoelectrochemical reduction of CO_2 coupled to water oxidation using a photocathode with a Ru(II)–Re(I) complex photocatalyst and a CoO_x/TaON photoanode. *J. Am. Chem. Soc.* **138**, 14152–14158 (2016).

13. Kumagai, H. *et al*. Hybrid photocathode consisting of a $CuGaO_2$ p-type semiconductor and a Ru(II)–Re(I) supramolecular photocatalyst: Non-biased visible-light-driven CO_2 reduction with water oxidation. *Chem. Sci.* **8**, 4242–4249 (2017).

14. Nakada, A. *et al*. Solar water oxidation by a visible-light-responsive tantalum/nitrogen-codoped rutile titania anode for photoelectrochemical water splitting and carbon dioxide fixation. *ChemPhotoChem* **3**, 37-45 (2019).

15. Wang, Q. *et al*. Particulate photocatalyst sheets based on carbon conductor layer for efficient Z-scheme pure-water splitting at ambient pressure. *J. Am. Chem. Soc.* **139**, 1675–1683 (2017).

16. Pinaud, B. A. *et al*. Technical and economic feasibility of centralized facilities for solar hydrogen production via photocatalysis and photoelectrochemistry. *Energy Environ. Sci.* **6**, 1983–2002 (2013).

17. Lian, S., Kodaimati, M. S., Dolzhnikov, D. S., Calzada, R. & Weiss, E. A. Powering a CO_2 reduction catalyst with visible light through multiple sub-picosecond electron transfers from a quantum dot. *J. Am. Chem. Soc.* 139, 8931–8938 (2017).

18. Rao, H., Schmidt, L. C., Bonin, J. & Robert, M. Visible-light-driven methane formation from CO_2 with a molecular iron catalyst. *Nature* **548**, 74–77 (2017).

19. Cometto, C. *et al*. A carbon nitride/Fe quaterpyridine catalytic system for photostimulated CO_2-to-CO conversion with visible light. *J. Am. Chem. Soc.* **140**, 7437–7440 (2018).

20. Li, P. *et al*. All-solid-state Z-scheme system arrays of $Fe_2V_4O_{13}$/RGO/CdS for visible light-driving photocatalytic CO_2 reduction into renewable hydrocarbon fuel. *Chem. Commun.* **51**, 800–803 (2015).

21. Iwase, A. *et al*. Water splitting and CO_2 reduction under visible light irradiation using Z-scheme systems consisting of metal sulfides, CoO_x-loaded $BiVO_4$, and a reduced graphene oxide electron mediator. *J. Am. Chem. Soc.* **138**, 10260–10264 (2016).

22. Suzuki, T. M. *et al*. Z-schematic and visible-light-driven CO_2 reduction using H_2O as an electron donor by a particulate mixture of a Ru-complex/$(CuGa)_{1-x}Zn_{2x}S_2$ hybrid catalyst, $BiVO_4$ and an electron mediator. *Chem. Commun.* **54**, 10199–10202 (2018).

23. Li, X., Yu, J., Jaroniec, M. & Chen, X. Cocatalysts for selective photoreduction of CO_2 into solar fuels. *Chem. Rev.* **119**, 3962–4179 (2019).

24. Wang, Q. *et al*. Scalable water splitting on particulate photocatalyst sheets with a solar-to-hydrogen energy conversion efficiency exceeding 1%. *Nat. Mater.* **15**, 611–615 (2016).

25. Minegishi, T., Nishimura, N., Kubota, J. & Domen, K. Photoelectrochemical properties of $LaTiO_2N$ electrodes prepared by particle transfer for sunlight-driven water splitting. *Chem. Sci.* **4**, 1120–1124 (2013).

26. Lin, F. *et al*. Photocatalytic oxidation of thiophene on $BiVO_4$ with dual co-catalysts Pt and RuO_2 under visible light irradiation using molecular oxygen as oxidant. *Energy Environ. Sci.* **5**, 6400–6406 (2012).

27. Ma, X. *et al*. Surface photovoltage spectroscopy observes sub-band-gap defects in hydrothermally synthesized $SrTiO_3$ nanocrystals. *J. Phys. Chem. C* **123**, 25081–25090 (2019).

28. Leung, J. J. *et al*. Solar-driven reduction of aqueous CO_2 with a cobalt bis(terpyridine)-based photocathode. *Nat. Catal.* **2**, 354–365 (2019).

29. Kudo, A., Omori, K. & Kato, H. A novel aqueous process for preparation of crystal form-controlled and highly crystalline $BiVO_4$ powder from layered vanadates at room temperature and its photocatalytic and photophysical properties. *J. Am. Chem. Soc.* **121**, 11459–11467 (1999).

30. Chang, X. *et al.* Enhanced surface reaction kinetics and charge separation of p−n heterojunction $Co_3O_4/BiVO_4$ Photoanodes. *J. Am. Chem. Soc*. **137**, 8356−8359 (2015).

31. Bassegoda, A., Madden, C., Wakerley, D. W., Reisner, E. & Hirst. J. Reversible interconversion of CO_2 and formate by a molybdenum-containing formate dehydrogenase. *J. Am. Chem. Soc.* **136**, 15473–15476 (2014).

32. Wakerley, D. W. & Reisner, E. Oxygen-tolerant proton reduction catalysis: Much O_2 about nothing? *Energy Environ. Sci.* **8**, 2283–2295 (2015).

33. Ryu, J., T. N. Andersen, T. N. & Eyring, H. The electrode reduction kinetics of carbon dioxide in aqueous solution. *J. Phys. Chem.* **76**, 3278–3286 (1972).

34. Akira, M. & Yoshio, H. Product selectivity affected by cationic species in electrochemical reduction of CO_2 and CO at a Cu electrode. *Bull. Chem. Soc. Jpn.* **64**, 123–127 (1991).

35. Pérez-Gallent, E., Marcandalli, G., Figueiredo, M. C., Calle-Vallejo, F. & Koper, M. T. M. Structure- and potential-dependent cation effects on CO reduction at copper single-crystal electrodes. *J. Am. Chem. Soc.* **139**, 16412–16419 (2017).

36. Feng, S. *et al.* Enriched surface oxygen vacancies of photoanodes by photoetching with enhanced charge separation. *Angew. Chem. Int. Ed.* **59**, 2044–2048 (2020).

37. Hykaway, N., Sears, W. M., Morisaki, H. & Morrison, S. R. Current-doubling reactions on titanium dioxide photoanodes. *J. Phys. Chem.* **90**, 6663–6667 (1986).

38. Sekizawa, K., Sato, S., Arai, T. & Morikawa, T. Solar-driven photocatalytic CO_2 reduction in water utilizing a ruthenium complex catalyst on p□type Fe_2O_3 with a multiheterojunction. *ACS Catal.* **8**, 1405−1416 (2018).

39. Leung, J. J., Vigil, J. A., Warnan, J., Edwardes Moore, E. & Reisner, E. Rational design of polymers for selective CO_2 reduction catalysis. *Angew. Chem. Int. Ed.* **58**, 7697–7701 (2019).

40. Belanger, D. & Jean Pinson, J. Electrografting: a powerful method for surface modification. *Chem. Soc. Rev.* **40**, 3995–4048 (2011).

41. Q. Wang, *et al.* Z-scheme water splitting using particulate semiconductors immobilized onto metal layers for efficient electron relay. *J. Catal.* **328**, 308–315 (2015).

42. Iwase, A., Ng, Y. H., Ishiguro, Y., Kudo, A. & Amal, R. Reduced graphene oxide as a solid-state electron mediator in Z-scheme photocatalytic water splitting under visible light. *J. Am. Chem. Soc.* **133**, 11054–11057 (2011).

43. Reisner E., *et al.* Data set for Molecularly engineered photocatalyst sheet for scalable solar formate production from carbon dioxide and water. *Cambridge Data Repository* https://doi.org/10.17863/CAM.54840 (2020)

44. Sasaki, Y., Iwase, A., Katoa, H. & Kudo, A. The effect of co-catalyst for Z-scheme photocatalysis systems with an Fe^{3+}/Fe^{2+} electron mediator on overall water splitting under visible light irradiation. *J. Catal.* **259**, 133–137 (2008).

Figure 1 | CotpyP-loaded $SrTiO_3$:La,Rh|Au|RuO_2-$BiVO_4$:Mo photocatalyst sheet. a, Energy diagram depicting photosynthetic CO_2RR coupled with water oxidation. **b,** Photograph of a 6 cm × 5.7 cm **CotpyP**-loaded $SrTiO_3$:La,Rh|Au|RuO_2-$BiVO_4$:Mo photocatalyst sheet prepared by the particle transfer method. **c – h,** Top-view SEM–EDX elemental mapping images showing a superimposition (**c**) of the distributions of Sr (**d**), Bi (**e**), Co (**f**), Ru (**g**), and Au (**h**).

Figure 2 | Photosynthetic activity of the CotpyP-loaded $SrTiO_3$:La,Rh|Au|RuO_2-$BiVO_4$:Mo sheet for CO_2RR coupled to water oxidation under AM 1.5G irradiation. a, A typical time course of the photosynthetic $HCOO^-$, O_2, H_2 and CO production on a **CotpyP**-loaded $SrTiO_3$:La,Rh|Au|RuO_2-$BiVO_4$:Mo sheet (ca. 1 cm^2). The dashed lines are guides to the eye. **b,** ^1H NMR spectra (D_2O, 500 MHz) of the solution after 6-hour irradiation using $^{12}CO_2/H^{12}CO_3^-$ (orange line, top) and $^{13}CO_2/H^{13}CO_3^-$ (green line, bottom) as reactants. **c,** Dependence of AQY for $HCOO^-$ production over the sheet on incident light wavelength, along with DRS of $SrTiO_3$:La,Rh (green line) and $BiVO_4$:Mo (orange line) for comparison. The blue dots indicate the AQYs of the system at various incident light wavelength. The error bars indicate the incident wavelength with a full width at half maximum of 15 nm. The reactions were carried out in a CO_2-saturated $KHCO_3$ aqueous solution (0.1 M, pH 6.7) under a CO_2 atmosphere (1 atm).

Figure 3 | CotpyP-loaded $SrTiO_3$:La,Rh|Au|RuO_2-$BiVO_4$:Mo photocatalyst sheet with an active irradiated area of ca. 20 cm^2 for photosynthetic CO_2RR coupled with water oxidation. a, Photograph of the sheet illuminated with simulated sunlight (AM 1.5G, 100 mW cm^{-2}). **b,** Time course of the photosynthetic CO_2RR and water oxidation over the sheet. The dashed lines are guides to the eye. The reaction was carried out in a CO_2-saturated 0.1 M $KHCO_3$ aqueous solution (180 mL, pH 6.7) without sacrificial reagents.

Figure 4 | Selectivity and stability of the CotpyP-loaded $SrTiO_3$:La,Rh|Au|RuO_2-$BiVO_4$:Mo sheet for CO_2RR coupled with water oxidation. a, Typical current-potential curves for a bare $SrTiO_3$:La,Rh|Au photoelectrode (orange curve) and a **CotpyP**-$SrTiO_3$:La,Rh|Au photoelectrode (green curve). **b,** Typical chronoamperometric curves of the **CotpyP**-$SrTiO_3$:La,Rh|Au photoelectrodes at an applied potential of 0.0 V (red line) and +0.5 V (blue line) versus RHE. The active areas of the photoelectrodes are ~0.2 cm^2. **c,** Dependence of the product distribution on **CotpyP**-modified and bare $SrTiO_3$:La,Rh|Au photocathodes on the applied potential after an experimental runtime of 4 h. The active areas of the photoelectrodes are ~0.2 cm^2. Error bars correspond to the standard deviation (n = 3). **d,** Time course of CO_2RR on a sheet for 30 hours, with complete replacement of the reactant media and CO_2 purging every 6 hours (dash-dotted black lines) and reloading of the **CotpyP** cocatalyst in the last run. The "1st, 2nd, 3rd and 4th" indicate the number of reaction cycles. The dashed lines are guides to the eye. All the above experiments were carried out in a CO_2-saturated $KHCO_3$ aqueous solution (0.1 M, pH 6.7) under a CO_2 atmosphere (1 atm) under simulated solar irradiation (AM 1.5G, 100 mW cm^{-2}).

Figure 5 | O_2-tolerance of CotpyP catalyst. a, LSV scans of a **CotpyP**|m-TiO_2|Ti electrode under CO_2+N_2 atmosphere (dark blue and dark red solid lines). The dark blue and dark red solid lines indicate the LSV recorded before and after 5 h of CPE carried out in CO_2+O_2, respectively. LSV scans of **CotpyP**|m-TiO_2|Ti recorded under CO_2+O_2 atmosphere (orange solid line), along with LSV scans of m-TiO_2|Ti under CO_2+N_2 atmosphere (black dash line) and CO_2+O_2 atmosphere (red dash line) are presented for comparison. The scans were recorded in an aqueous $KHCO_3$ solution (0.1 M, pH 6.7) and dark condition at a scan rate of 50 mV s^{-1}. **b,** *J-t* traces from the first 5 hours of CPE with **CotpyP**|m-TiO_2|Ti under a CO_2+N_2 atmosphere (red trace) and CO_2+O_2 atmosphere (blue trace) at an applied potential of –0.3 V versus RHE.

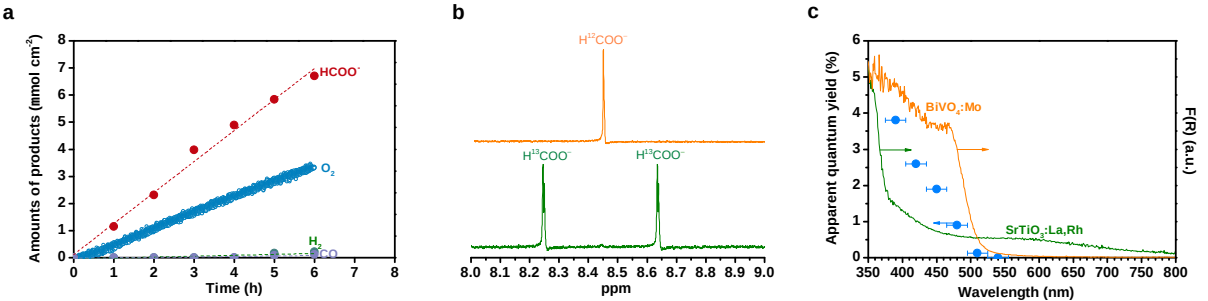
a
Amounts of products (mmol cm^{-2})
Time (h)
HCOO$^-$
O_2
H_2
CO
b
$H^{13}COO^-$
$H^{13}COO^-$
$H^{13}COO^-$
ppm
c
Apparent quantum yield (%)
F(R) (a.u.)
Wavelength (nm)
$BiVO_4$:Mo
$SrTiO_3$:La,Rh

a

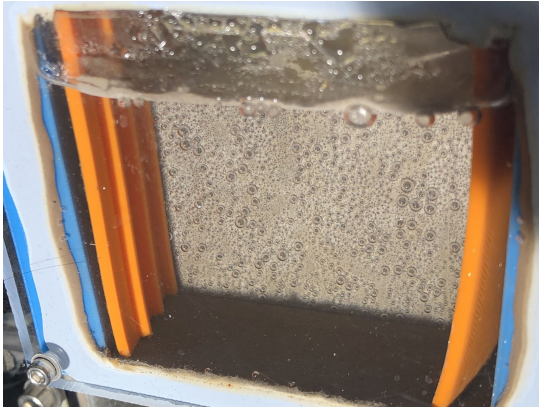

b

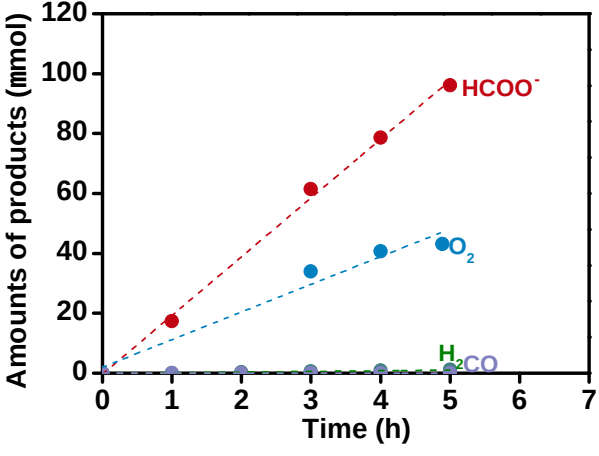
Amounts of products (mmol)
120
100
80
60
40
20
0
0
1
2
3
4
5
6
7
Time (h)
HCOO-
O2
H2
CO

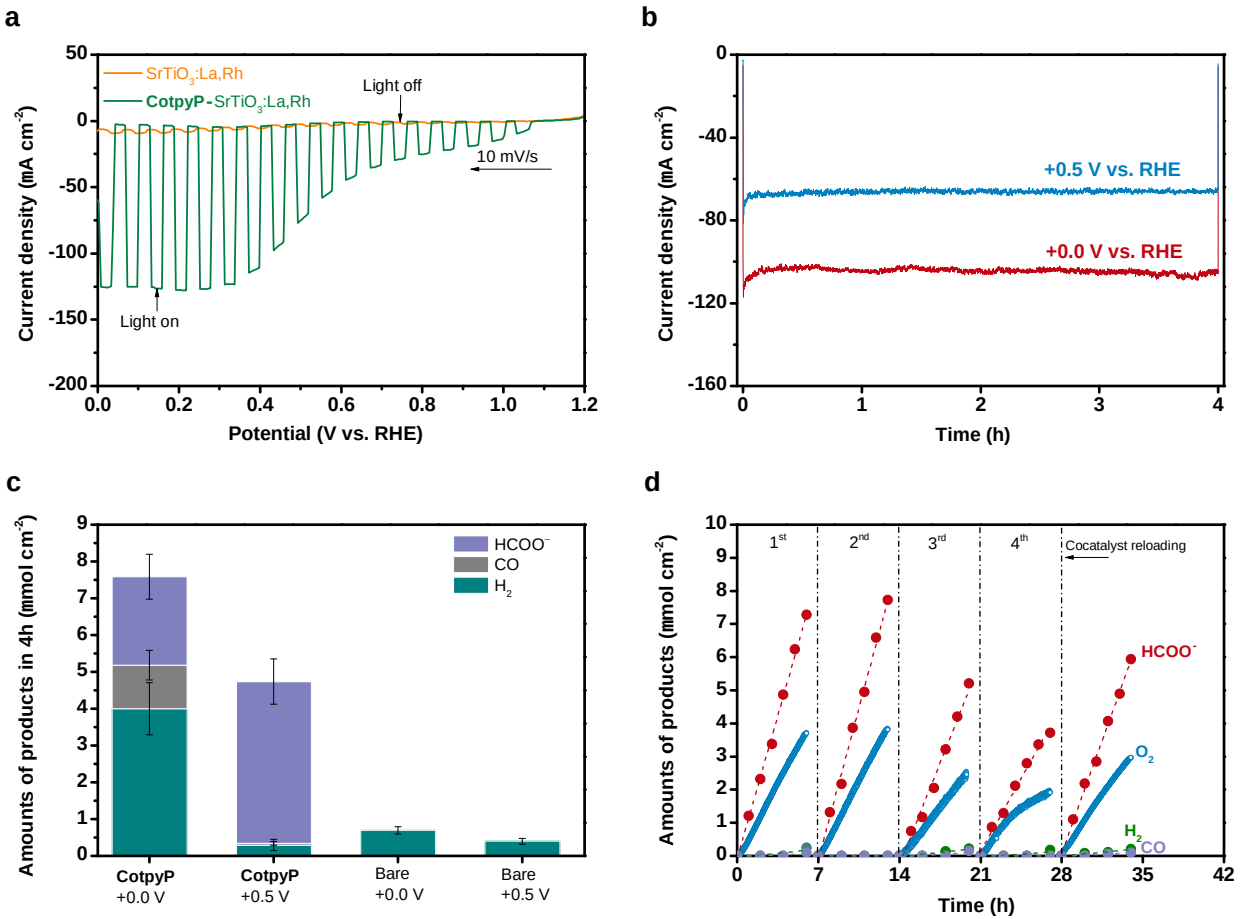
a
SrTiO3:La,Rh
CotpyP-SrTiO3:La,Rh
Light off
10 mV/s
Light on
Current density (mA cm-2)
Potential (V vs. RHE)
b
+0.5 V vs. RHE
+0.0 V vs. RHE
Current density (mA cm-2)
Time (h)
c
HCOO-
CO
H2
Amounts of products in 4h (mmol cm-2)
CotpyP +0.0 V
CotpyP +0.5 V
Bare +0.0 V
Bare +0.5 V
d
1st
2nd
3rd
4th
Cocatalyst reloading
HCOO-
O2
H2
CO
Amounts of products (mmol cm-2)
Time (h)

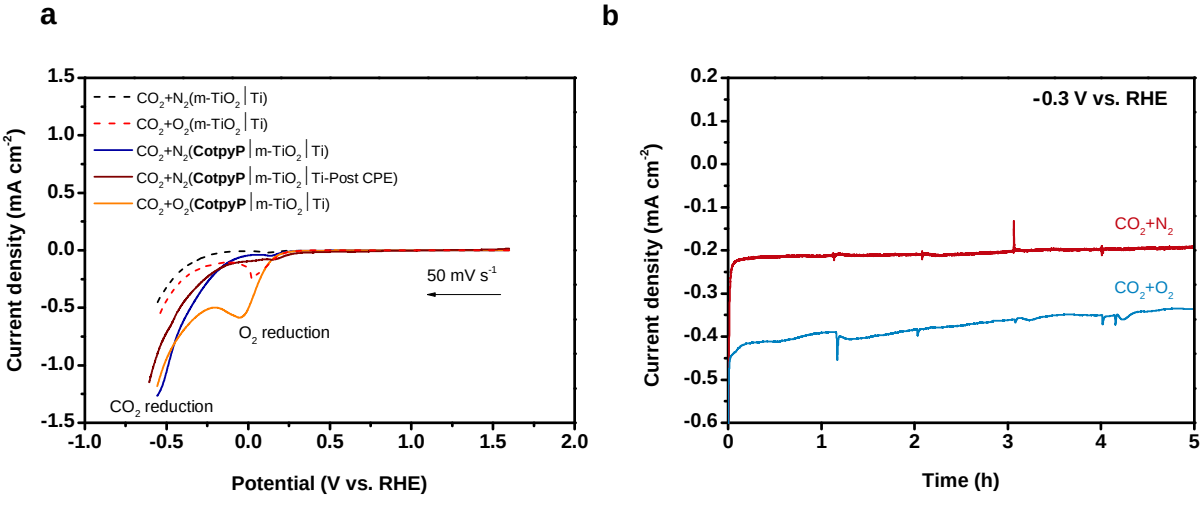
a
b
CO2+N2(m-TiO2 | Ti)
CO2+O2(m-TiO2 | Ti)
CO2+N2(CotpyP | m-TiO2 | Ti)
CO2+N2(CotpyP | m-TiO2 | Ti-Post CPE)
CO2+O2(CotpyP | m-TiO2 | Ti)
50 mV s-1
O2 reduction
CO2 reduction
Current density (mA cm-2)
Potential (V vs. RHE)
-0.3 V vs. RHE
CO2+N2
CO2+O2
Time (h)

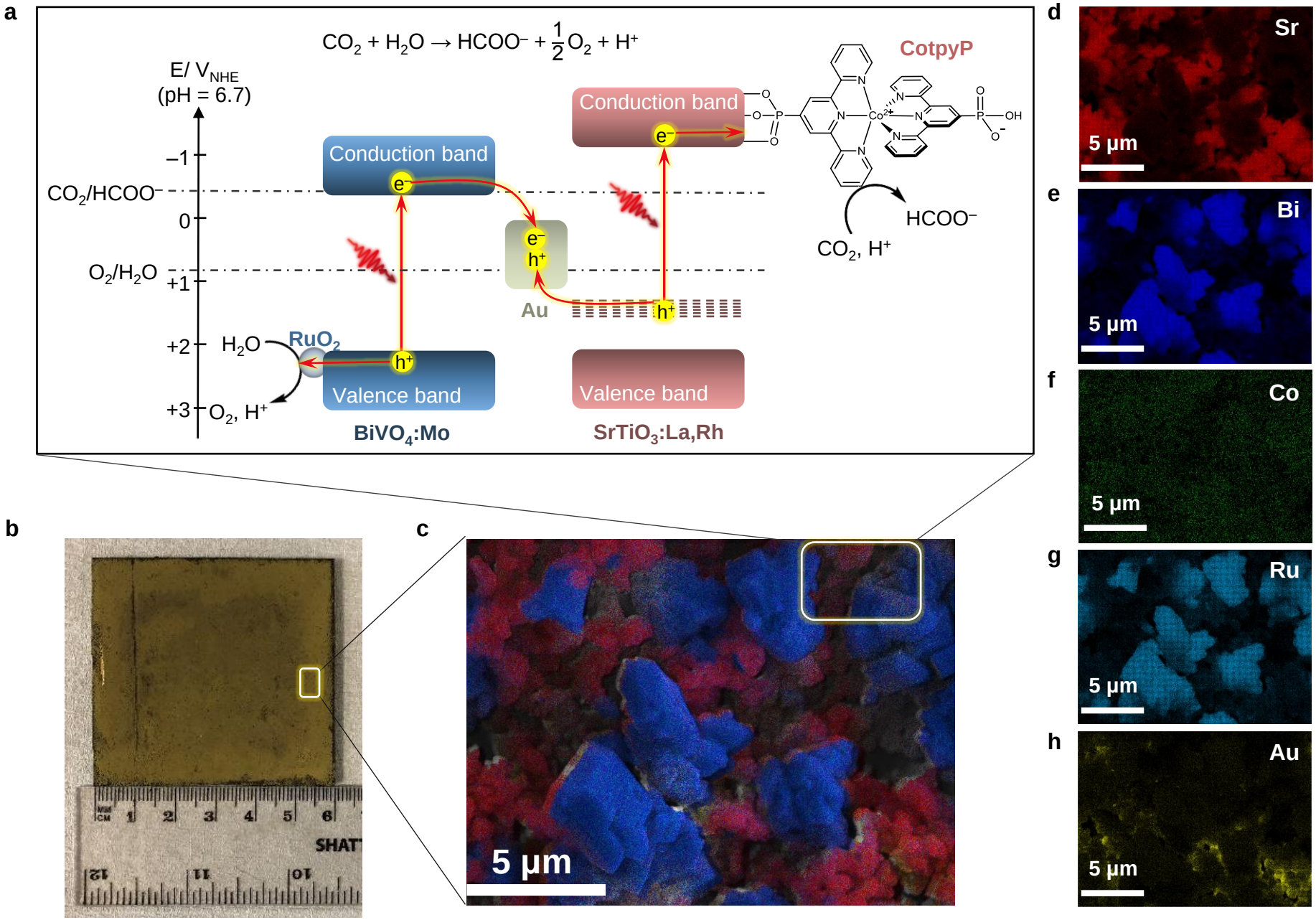
a
$CO_2 + H_2O \rightarrow HCOO^- + \frac{1}{2}O_2 + H^+$
E/ V_{NHE}
(pH = 6.7)
–1
$CO_2/HCOO^-$
0
O_2/H_2O
+1
+2
+3
H_2O
RuO_2
O_2, H^+
Conduction band
Valence band
$BiVO_4$:Mo
Au
Conduction band
Valence band
$SrTiO_3$:La,Rh
CotpyP
$HCOO^-$
CO_2, H^+
b
c
5 µm
d
Sr
5 µm
e
Bi
5 µm
f
Co
5 µm
g
Ru
5 µm
h
Au
5 µm